Biochimica et Biophysica Acta 1840 (2014) 2080–2090

Contents lists available at ScienceDirect

Biochimica et Biophysica Acta

journal homepage: www.elsevier.com/locate/bbagen

Tetracycline nanoparticles loaded calcium sulfate composite beads for periodontal management

N. Sindhura Reddy [a,1], S. Sowmya [a,1], Joel D. Bumgardner [b], K.P. Chennazhi [a], Raja Biswas [a], R. Jayakumar [a,*]

[a] Amrita Centre for Nanosciences and Molecular Medicine, Amrita Institute of Medical Sciences and Research Centre, Amrita Vishwa Vidyapeetham University, Kochi 682041, India
[b] Biomedical Engineering Department, University of Memphis, Joint University of Memphis–University of Tennessee Graduate Biomedical Engineering Program, Memphis, TN, USA

ARTICLE INFO

Article history:
Received 16 November 2013
Received in revised form 31 January 2014
Accepted 10 February 2014
Available online 18 February 2014

Keywords:
Calcium sulfate
Tetracycline nanoparticles
Antibacterial
Cytocompatible
Periodontal regeneration

ABSTRACT

Background: The objective of this study was to fabricate, characterize and evaluate in vitro, an injectable calcium sulfate bone cement beads loaded with an antibiotic nanoformulation, capable of delivering antibiotic locally for the treatment of periodontal disease.
Methods: Tetracycline nanoparticles (Tet NPs) were prepared using an ionic gelation method and characterized using DLS, SEM, and FTIR to determine size, morphology, stability and chemical interaction of the drug with the polymer. Further, calcium sulfate ($CaSO_4$) control and $CaSO_4$-Tet NP composite beads were prepared and characterized using SEM, FTIR and XRD. The drug release pattern, material properties and antibacterial activity were evaluated. In addition, protein adsorption, cytocompatibility and alkaline phosphatase activity of the $CaSO_4$-Tet NP composite beads in comparison to the $CaSO_4$ control were analyzed.
Results: Tet NPs showed a size range of 130 ± 20 nm and the entrapment efficiency calculated was 89%. The composite beads showed sustained drug release pattern. Further the drug release data was fitted into various kinetic models wherein the Higuchi model showed higher correlation value ($R^2 = 0.9279$) as compared to other kinetic models. The composite beads showed antibacterial activity against *Staphylococcus aureus* and *Escherichia coli*. The presence of Tet NPs in the composite bead didn't alter its cytocompatibility. In addition, the composite beads enhanced the ALP activity of hPDL cells.
Conclusions: The antibacterial and cytocompatible $CaSO_4$-Tet NP composite beads could be beneficial in periodontal management to reduce the bacterial load at the infection site.
General significance: Tet NPs would deliver antibiotic locally at the infection site and the calcium sulfate cement, would itself facilitate tissue regeneration.

1. Introduction

Periodontal disease causes severe inflammation, alveolar bone loss, tooth mobility, tooth loss and other serious complications if left untreated. Replacement of bone loss due to inefficient bone healing, and controlling the microbial infections are some of the noteworthy clinical challenges [1]. The main goal of treating the periodontal infections includes the reduction of bacterial load at the infection site which if left unattended may delay healing and affect new bone formation and periodontal ligament re-attachment [1,2]. The conventional treatment procedures involve the systemic delivery of high dosage antibiotics; however these led to systemic toxicities of the liver. In order to avoid such toxicity issues, and to improve the prognosis of the patients with such infections, local antibiotic delivery systems were developed. The main reason for using such local antibiotic delivery vehicles is the ability to achieve very high local concentrations of antibiotics without associated systemic toxicity [3,4]. Initially, studies used non-biodegradable bone cements with materials like poly(methyl methacrylate) (PMMA) [5–7], however these bone cements had one major disadvantage of requiring a second surgical intervention solely for their removal [8]. In order to avoid such disadvantages, the use of biodegradable materials, both natural and synthetic, came into play [9]. Ceramics are widely used as bone cements for the repair and reconstruction of diseased and damaged

Abbreviations: ALP, alkaline phosphatase; BCA, bicinchoninic acid; *O*-CMC, *O*-carboxymethyl chitosan; $CaCl_2$, calcium chloride; $CaSO_4$, calcium sulfate; $CaSO_4 \cdot 1/2H_2O$, calcium sulfate hemihydrate; CFU, colony forming units; DAPI, 4′,6-diamidino-2-phenylindole; DD, degree of deacetylation; DLS, dynamic light scattering; *E. coli*, *Escherichia coli*; EthD-1, ethidium homodimer-1; EtO, ethylene oxide gas; FBS, fetal bovine serum; FTIR, Fourier transform infrared spectroscopy; HAp, hydroxyapatite; hPDL, human periodontal ligament cells; L.B. broth, Luria Bertani broth; MEM, minimal essential media; NPs, nanoparticles; PBS, phosphate buffered saline; Pen–Strep, penicillin–streptomycin; PNPP, *p*-nitrophenylphosphate; K_2SO_4, potassium sulfate; SEM, scanning electron microscope; *S. aureus*, *Staphylococcus aureus*; Tet, tetracycline hydrochloride; XRD, X-ray diffraction

* Correspondence author at: Amrita Centre for Nanosciences and Molecular Medicine, Amrita Institute of Medical Sciences and Research Centre, Amrita Vishwa Vidyapeetham University, Kochi 682041, India. Tel.: +91 484 2801234; fax: +91 484 2802020.
E-mail addresses: rjayakumar@aims.amrita.edu, jayakumar77@yahoo.com (R. Jayakumar).
[1] Both the authors have contributed equally.

http://dx.doi.org/10.1016/j.bbagen.2014.02.007
0304-4165/

parts of the body, and are generally termed as bioceramics. The most widely used bioceramics are calcium phosphate [10], and calcium sulfate [11]. Though calcium phosphate has been widely used as a bone void filler, calcium sulfate is a better option because of its biodegradable nature (resorption rate of calcium phosphate is very slow) [10].

Calcium sulfate hemihydrate ($CaSO_4 \cdot 1/2H_2O$) commonly known as Plaster of Paris has been used as a bone void filler since 1928. The increasing attention to calcium sulfate being used as bone cement is largely due to its biodegradable, biocompatible, and its injectable nature. It is also characterized by osteointegrity and new bone formation ability [11]. The dissolution property of calcium sulfate makes it possible to be used for drug release, such as antibiotics [11–14]. In addition, the dissolution rate of calcium sulfate in comparison to calcium phosphate can exceed the ability for new bone formation. However, the mechanical characteristics for most calcium sulfate compounds, show low compressive strength and a brittle appearance, thus are generally applicable to small bone defects [15].

Antibiotics such as tetracyclines, a group of broad spectrum antibiotics, exhibit activity against both gram positive as well as gram negative bacteria, and are clinically very efficient in controlling periodontal bone infections [16]. They are generally bacteriostatic in nature. Tetracycline (Tet) shows its antibacterial activity by entering through the bacterial cell wall and reversibly binding to the 30S ribosomal subunit thereby inhibiting protein synthesis and leads to bacteriostatic effect. In addition, Tet also reduces the inflammation at the infection site by blocking a protein, collagenase that destroys bone and other connective tissues [16,17].

In contrast to the work so far published, drug-nanoparticle based composite cement beads were developed to obtain the necessary antibacterial effect to treat bacterial infections and promote tissue regeneration. These drug based nanoparticles would help us to achieve the desired antibacterial effect at the lowest possible dosage of the drug. Besides drug encapsulation, polymeric nanoparticle is a well suited vehicle for antimicrobial drug delivery that allows sustained release of the drug, minimizes the toxicity associated with the conventional administration of bare drug and increases the bioavailability of the drug [18]. In the present study we have developed Tet-*O*-CMC NPs using *O*-carboxymethyl chitosan (*O*-CMC) with calcium chloride ($CaCl_2$) as a cross-linking agent. *O*-CMC has been widely used as the sustained drug-release carrier in pharmaceutical field and acts as a good antibiotic carrier. *O*-CMC is very advantageous due to its non-toxicity, biodegradability, biocompatibility, antibacterial, antifungal and bioactivity and therefore is a promising polymer derivative for bio-medical applications [19–21]. These Tet-*O*-CMC NPs (at minimal concentration of 2 wt.%) in the composite beads would maintain a local concentration of the drug with an extended duration of release without exceeding systemic toxicity thereby ensuing the necessary antibacterial effect [18,22]. Consecutively, the calcium sulfate on degradation/dissolution would promote bone tissue regeneration.

Hence the objective of this study was to fabricate a delivery system with ceramic bone cement, wherein, calcium sulfate loaded with antibiotic tetracycline nanoformulation would deliver tetracycline locally to achieve the required antibacterial effect. In addition, the bone cement would itself facilitate tissue regeneration.

2. Materials and methods

2.1. Materials

O-CMC (degree of deacetylation — 61.8% and degree of substitution — 0.54) was purchased from Koyo Chemical Co. Ltd. Japan, calcium chloride ($CaCl_2$), minimum essential medium (MEM), Triton X-100, paraformaldehyde, *p*-nitrophenylphosphate (PNPP) and potassium sulfate (K_2SO_4) were purchased from SIGMA Aldrich Company, calcium sulfate ($CaSO_4$) from Fischer Scientific, tetracycline hydrochloride (Tet), *Staphylococcus aureus* (*S. aureus*) (ATCC 25923) and *Escherichia coli* (*E. coli*) (ATCC 25922) strains were provided by Microbiology Lab of Amrita Institute of Medical Sciences, Kochi, India. Luria Bertani broth (L.B. broth), agar–agar and alkaline phosphatase (ALP) were purchased from Himedia, India. Human periodontal ligament cells (hPDL) were obtained from Science Cell, USA. Glutaraldehyde was purchased from Fluka. Alamar blue, trypsin-EDTA, DAPI (4′, 6-diamidino-2-phenylindole), penicillin–streptomycin (Pen–Strep), fetal bovine serum (FBS), acridine orange and ethidium bromide were obtained from Gibco, Invitrogen Corporation. All chemicals were used as such with no further purification.

2.2. Preparation and characterization of Tet-O-CMC NPs

0.1% *O*-CMC solution was prepared as reported in literature [23]. 0.001% tetracycline (Tet) solution was prepared by dissolving Tet in ethanol–water mixture. This 0.001% Tet solution was added to 0.1% *O*-CMC solution in a ratio of 5:10 under constant stirring for 4 h. The solution was further cross-linked using 0.05% $CaCl_2$ solution that was added dropwise under continuous stirring until the formation of an opalescent suspension was observed [19]. The reaction of the Ca^{2+} ions (of the cross-linking agent) with the carboxyl group (of *O*-CMC) yielded tetracycline-carboxymethyl chitosan nanoparticles (Tet-*O*-CMC NPs) [22]. The NP suspension thus obtained was purified by centrifugation for 15 min at 15,000 rpm, lyophilized and used for further studies [19].

The particle size distribution of the NPs (in triplicates) was analyzed using dynamic light scattering (Malvern Zeta Sizer, Nano Series) and morphological evaluation was performed using a scanning electron microscope (JEOL JSM-6490LA Analytical SEM). The potential interactions between the constituents of the nanoparticle system (in triplicates) were analyzed using Fourier transform infrared spectroscopy (PerkinElmer Co, SPECTRUM RX1, FTIR).

2.3. Entrapment efficiency

The entrapment efficiency and loading efficiency were determined as reported in the literature [19,24]. It was calculated using the formula:

$$\text{Entrapment efficiency}(\%) = \frac{\text{Total amount of Tet added} - \text{Free Tet}}{\text{Total amount of Tet added}} \times 100$$

$$\text{Loading efficiency}(\%) = \frac{\text{Total amount of Tet}}{\text{Total amount of nanoparticles}} \times 100.$$

2.4. Preparation and characterization of $CaSO_4$ control and $CaSO_4$-Tet NP composite beads

100 mg of calcium sulfate ($CaSO_4$) was thoroughly mixed with required quantity of 3% potassium sulfate (K_2SO_4) solution to obtain a paste [25]. The paste was further molded into spherical bead form which served as the $CaSO_4$ control beads. For the composite beads, 2 wt.% of lyophilized Tet-*O*-CMC or Tet NPs (~89% encapsulation efficiency and 48% loading efficiency, wherein, the Tet quantity was found to be ~1 wt.%) were mixed with 100 mg $CaSO_4$ and 3% K_2SO_4 solution to obtain a paste further molded into spherical beads of 1 mm diameter. Several such beads were prepared for analytical and *in vitro* studies. These beads would facilitate periodontal regeneration by reducing gingival inflammation (gums) followed by restoration of normal alveolar bone level and periodontal ligament fibers in the affected area.

The structural morphology of the $CaSO_4$ control and $CaSO_4$-Tet NPs composite beads (in triplicates) was analyzed by SEM. The presence of Tet NPs in the composite bead (in triplicates) was confirmed through X-ray diffraction (XRD) (PAN analytical X'Pert PRO X-ray diffractometer) and FTIR analysis.

2.5. Porosity study

Porosity of the $CaSO_4$ control and $CaSO_4$-Tet NP composite beads was determined by liquid displacement method [26]. The dimensions of triplicate set of beads, both the control and sample, were measured with a vernier caliper and their corresponding volumes were calculated. Following, the beads were immersed in 100% ethanol for 48 h until saturation, and the porosity was calculated using the formula:

$$P = \frac{(W_2 - W_1)}{\rho V}$$

where,

W_1 initial weight of the bead before immersing in ethanol,
W_2 the weight of the bead after immersing in ethanol,
V volume of the bead before immersing,
ρ a constant of the density of ethanol.

Porosity was expressed as mean ± SD (n = 3).

2.6. Swelling study

The swelling study was performed in distilled water at 37 °C as reported previously [27]. The $CaSO_4$ control and $CaSO_4$-Tet NP composite beads were placed in distilled water and incubated at 37 °C for different time durations such as 1, 7, 14 and 21 days respectively. The swelling ratio was determined using the formula:

$$\text{Swelling ratio} = \frac{W_w - W_d}{W_d}$$

where,

W_w wet weight of the bead
W_d dry weight of the bead.

Swelling ratio was expressed as mean ± SD (n = 3).

2.7. In vitro biodegradation study

The *in vitro* biodegradation of both the $CaSO_4$ control and $CaSO_4$-Tet NP composite beads was carried out in PBS (pH 7.4) at 37 °C (100 mg of bead to 3 ml of PBS) as reported previously [27,28]. The degradation % was calculated using the formula:

$$\%\text{Degradation} = \frac{W_{d1} - W_{d2}}{W_{d1}} \times 100$$

where,

W_{d1}: initial dry weight
W_{d2}: dry weight after the desired time interval.

Degradation rate was expressed as mean ± SD (n = 3).

2.8. In vitro drug release study and it's kinetic modeling

The *in vitro* drug release studies were carried out at a pH of 7.4 [24,25]. The $CaSO_4$-Tet NP composite beads were soaked in phosphate buffered saline (PBS) (pH 7.4) and incubated at 37 °C under gentle shaking (100 mg of bead to 3 ml of PBS). A time dependent release study was carried out which was quantified using a UV–visible spectrophotometer at 270 nm by calculating the concentration of the released Tet. Drug release % was calculated using the formula:

$$\text{Drug release}(\%) = \frac{\text{Tet released at definite time}}{\text{Total amount of Tet in the bead}} \times 100.$$

The *in vitro* drug release was expressed as mean ± SD (n = 3).

Kinetic modeling is often helpful in elucidating release mechanisms which can be of use in the control of drug release [29]. To carry out the kinetic modeling study of *in vitro* drug release, the data obtained from *in vitro* drug release studies were plotted and data were fitted to various kinetic models representing zero order, first order, Higuchi model and Hixson–Crowell model (Table 1). Regression analysis was used to determine the kinetic model coefficient. The closeness of the regression coefficient to unity was assumed as the best fit kinetic model. To understand the drug release mechanism, the data were fitted into Korsmeyer–Peppas model, where the exponent 'n' value indicated the drug transport mechanism. Based on the n value, the mechanism of diffusion can be assessed (Table 2).

2.9. Antibacterial activity and bacterial live dead assay

Antibacterial activity of the $CaSO_4$ control and $CaSO_4$-Tet NP composite beads against gram positive *S. aureus* and gram negative *E. coli* was assessed. The bacterial strains were cultured in L.B. broth as reported in literature [30]. The control and composite beads (in triplicates) weighing 100 mg each were sterilized using EtO gas and placed in L.B. broth containing bacterial cells (1 bead in 10 ml L.B. broth) and incubated for 24 h at 37 °C. After incubation, 100 μl L.B. broth containing bacteria was serially diluted 10 times in sterile saline and plated onto L.B. agar plates. Finally the number of bacterial colonies was counted.

Antibacterial activity was expressed as mean CFU's ± SD (n = 3).

Further to assess the toxicity of the composite beads towards bacterial cells, live/dead staining was performed which is a fluorescence two-color cell viability assay, uses dyes acridine orange and ethidium bromide (EtBr), that simultaneously detects both the viable and non-viable bacterial cells based on the integrity of plasma membrane [31]. Triplicates of control and composite beads weighing 100 mg each, pre-sterilized using EtO gas were incubated in L.B. broth containing bacterial cells 1×10^6 CFU/ml (1 bead in 10 ml L.B. broth) for 24 h at 37 °C. 1 ml of broth added to Eppendorf tubes was separately stained with 2 μmol/l acridine orange and 4 μmol/l EtBr and incubated for 20 min at RT in dark. Subsequently, 100–200 μl of stained L.B. broth was placed on a glass slide and visualized using a fluorescence microscope (Olympus-BX-51).

2.10. Protein adsorption

Bicinchoninic acid (BCA) assay was performed to quantify the total protein adsorption onto the beads (100 mg each of similar shape and size) as reported earlier. Triplicates of $CaSO_4$ control and $CaSO_4$-Tet NP composite beads were placed in a 96 well plate and incubated at 37 °C with minimum essential media (MEM with a pH of 7.4) containing 10% fetal bovine serum (FBS) (in the absence of cells/bacteria) for 24 and 48 h respectively; rinsed with PBS solution twice after the predetermined incubation time and the beads were further incubated in elution buffer for 1 h at 37 °C prior to quantification using BCA assay [32]. As reported earlier, its principle is based on the reduction of Cu^{2+} to Cu^{1+}. The reduction corresponds to the amount of protein present. BCA reagent was added to each well and incubated for 30 min with the eluted extract at 37 °C and the absorbance was read at a wavelength of 562 nm. Scaffolds incubated in serum free medium were used as blank.

Protein adsorption was expressed as mean ± SD (n = 3).

Table 1
Drug release kinetic models.

1x Zero order rate kinetics	$Q_t = Q_0 - K_0t$	Q_0: initial of drug present in solution
2) First order rate kinetics	$\ln Q = \ln Q_0 - K_1t$	Q_t: amount of drug released at time t
3) Higuchi model	$Q = K_Ht^{1/2}$	K_0: zero order rate constant expressed in terms of unit time^{-1}
4) Hixon–Crowell model	$Q_0^{1/3} - Q_t^{1/3} = K_2t$	K_1: first order rate constant expressed in terms of unit time^{-1}
5) Korsmeyer Peppas Model	$Mt/M\alpha = K_Kt^n$	K_H: Higuchi dissolution constant
		K_2: constant incorporating the surface–volume relation Mt/Mα: fractional solute release
		K_K: kinetic constant
		n: exponent which indicates the mechanism of drug release
		t: time of hours

Table 2
Diffusion exponent (n) value to describe the diffusion mechanism.

Diffusion exponent (n)	Overall solute diffusion mechanism
0.45	Fickian diffusion
0.45 < n < 0.89	Non-Fickian diffusion
0.89	Case-II transport
n > 0.89	Super case-II transport

2.11. Cell viability evaluation

Alamar blue assay was performed to measure cellular viability of $CaSO_4$ control and $CaSO_4$-Tet NP composite beads [32,33]. Human periodontal ligament cells (hPDL) were cultured as reported earlier and seeded at a density of 10,000 cells/bead onto EtO sterilized control and composite beads placed in a 24 well plate and incubated in serum containing medium at 37 °C for 24 and 48 h respectively. The optical density (OD) at 570 and 600 nm was measured using a microplate reader (Biotek Power Wave XS, USA).

Cell viability was expressed as mean ± SD (n = 3).

2.12. Cell attachment and proliferation

The EtO sterilized $CaSO_4$ control and $CaSO_4$-Tet NP composite beads (in triplicates) were tested for hPDL cell attachment and proliferation as reported earlier [32,33]. After 24 h of incubation, the beads for cell attachment were examined using SEM. After 48 h of incubation, the beads for cell proliferation were stained using DAPI and viewed under a fluorescent microscope (Olympus-BX-51).

2.13. Alkaline phosphatase (ALP) activity

ALP activity was measured using a colorimetric endpoint assay that utilizes *p*-nitrophenol phosphate (PNPP) as the substrate. The EtO sterilized $CaSO_4$ control and $CaSO_4$-Tet NP composite beads were placed in a 24 well plate and the hPDL cells were seeded onto the beads (5×10^4 cells/bead) and incubated at 37 °C in a humidified incubator with 5% CO_2 and 85% humidity for 48 h, for the cells to attach and proliferate. After 4 h, the cell seeded beads were fed with serum containing medium. After 48 h, the medium was replaced with osteogenic medium (MEM, 10% FBS, 50 μg/ml L-ascorbic acid, 10 mM glycerophosphate and 100 nM dexamethasone) and incubated for a period of 7, 14 and 21 days. The osteogenic medium was changed once in every 3 days. After the pre-determined time interval, the medium was removed; beads were washed with PBS and incubated with 1% Triton X-100 for 2 h to obtain cell lysates which were ultrasonicated for 30 min. The supernatant thus obtained was incubated with PNPP substrate in the presence of glycine buffer (to maintain an alkaline pH) for 30 min in dark at 37 °C. The ALP activity corresponds to spectrophotometric endpoint which determines the conversion of colorless PNPP substrate into colored *p*-nitrophenol. Thus ALP activity is directly proportional to the *p*-nitrophenol end-product, and the further reaction was blocked by adding 5 M NaOH. Sample absorbance was measured at 405 and 490 nm. Standards were prepared from *p*-nitrophenol and ALP control.

The ALP activity was calculated as mean ± SD (n = 3).

2.14. Statistical analysis

All quantitative results were obtained from triplicate samples. Data was expressed as mean ± SD. Statistical analysis was carried out using Student's two-tailed *t*-test. A value of $p < 0.05$ was considered to be statistically significant.

3. Results

3.1. Characterization and entrapment efficiency of Tet NPs

The particle size distribution of Tet NPs (synthesized by ionic gelation method) determined by DLS showed particle size in the range of 148 ± 37 nm. SEM analysis (Fig. 1A) showed spherical shaped particles with a size range 130 ± 20 nm.

To ascertain the formation of Tet NPs, FTIR analysis was also performed. From the FTIR spectrum (Fig. 1B) it was evident that *O*-CMC depicts a broad peak at 3420 cm^{-1} due to stretching vibration of hydroxyl and amine groups. Stretching vibration of carbonyl and protonated amino groups was observed at 1740 and 1629 cm^{-1} and another peak at 1320 cm^{-1} corresponds to C – O stretching [19,24]. Bare Tet exhibited a high intensity peak at 3365 cm^{-1} which corresponds to C – N vibrations [34]. The ν(C═O) and ν(C═C) of the aromatic ring are observed between 1674 and 1580 cm^{-1} and the peaks which correspond to stretching of NH bonds and C – N bond vibrations are observed at 1240–1200 cm^{-1} [34]. The FTIR spectrum of Tet NP showed characteristic peak at 3500 cm^{-1}, a sharpened peak with a high intensity. Comparing the spectrums of bare *O*-CMC and Tet NPs, a shift in the peak corresponding to carboxyl group was noticed at 1674 cm^{-1} in bare *O*-CMC to 1610 cm^{-1} in Tet NPs [19]. These shifts in the IR spectrum confirm the conjugation of drug with the *O*-CMC matrix.

From the preparative conditions of the nanoformulation [19], the drug loading was optimized to 10:5 (polymer:drug) ratio and the encapsulation efficiency and loading efficiency were calculated as 89% and 48% respectively for Tet NPs.

3.2. Characterization of $CaSO_4$ control and $CaSO_4$-Tet NP composite beads

The morphology of prepared $CaSO_4$ control and $CaSO_4$-Tet NP composite beads was analyzed using SEM (Fig. 2A and B). The SEM image of $CaSO_4$ control beads showed the presence of long needle like morphology with a smooth surface. However in the $CaSO_4$-Tet NP composite beads, the smooth surface of $CaSO_4$ needles was altered by the presence of Tet NPs (spherical in shape).

The FTIR spectra of $CaSO_4$ control showed a broad peak in the range of 3405–3550 cm^{-1} which corresponds to O – H stretching

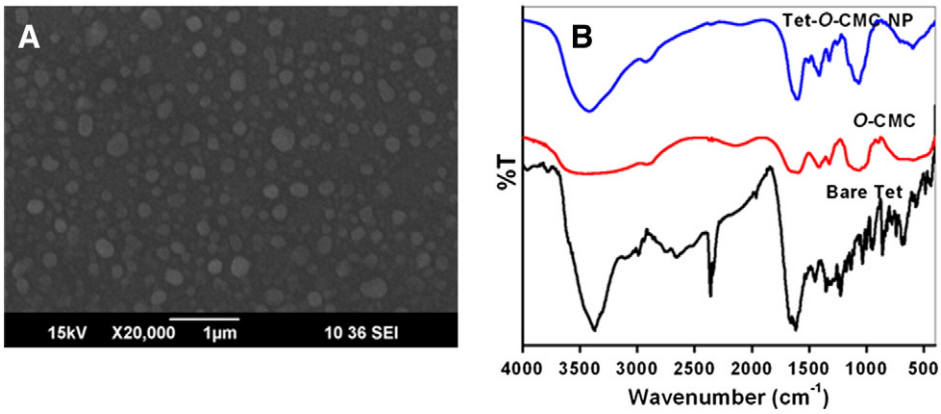

Fig. 1. (A) SEM image of Tet NPs showing the spherical morphology and size range of 130 ± 20 nm, (B) FTIR spectra of bare Tet, *O*-CMC and Tet NPs confirming the conjugation of Tet with the *O*-CMC matrix.

of the water molecules of crystallization. A peak observed in the range of 1622–1690 cm^{-1} is due to the O–H bending while the ones in the range of 600–660 cm^{-1} and 1111–1140 cm^{-1} correspond to S–O stretching and S–O bending respectively [35]. The spectra of $CaSO_4$-Tet NP composite bead showed a sharp peak at 3556 cm^{-1} in contrast to the $CaSO_4$ control spectra. Thus we could confirm the presence of Tet NPs in the $CaSO_4$ composite bead (Fig. 2C).

The XRD spectrum (Fig. 2D) showed that Tet NPs were amorphous in nature. $CaSO_4$ control showed characteristic crystalline peaks of 2θ at 15, 25, 30, 31 and 48° corresponding to (200), (020), (002), (102) and (302) planes respectively [36]. The XRD spectrum of $CaSO_4$-Tet NP composite bead showed reduced peak intensity as compared to the $CaSO_4$ control. This reduction in peak intensity could also be due to the amorphous nature of *O*-CMC in the Tet NPs.

3.3. Porosity, swelling and in vitro biodegradation study

Fig. 3A depicts the percentage porosity of the $CaSO_4$ control and $CaSO_4$-Tet NP composite beads in absolute ethanol. Composite beads showed around 44% porosity whereas the control beads showed a lower porosity of 19.8%. This significant increase in porosity could ideally support tissue regeneration functions.

Fig. 3B depicts the swelling (water uptake) behavior of the $CaSO_4$ control and $CaSO_4$-Tet NP composite beads at 37 °C. On day 1, the NP incorporated composite beads showed higher swelling ratio compared to the $CaSO_4$ control bead. Thereafter the swelling ratio of both the $CaSO_4$ control and $CaSO_4$-Tet NP composite beads was found to decrease.

Fig. 3C depicts the *in vitro* biodegradation profile of $CaSO_4$ control and $CaSO_4$-Tet NP composite beads in PBS (pH 7.4) at 37 °C. On days

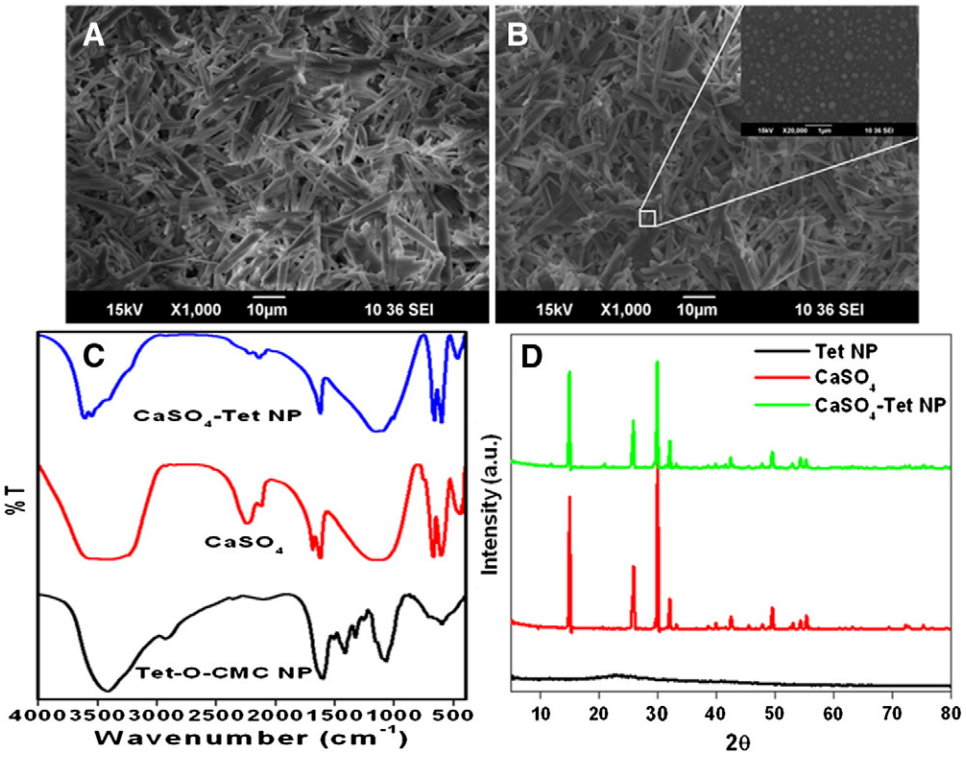

Fig. 2. (A) SEM image of $CaSO_4$ control bead showing needle-like morphology, (B) SEM image of $CaSO_4$-Tet NP composite bead (the inset shows Tet NPs in the $CaSO_4$ matrix), (C) FTIR spectra and (D) XRD spectra of Tet NPs, $CaSO_4$ control and $CaSO_4$-Tet NP composite beads showing the chemical interaction between the constituents.

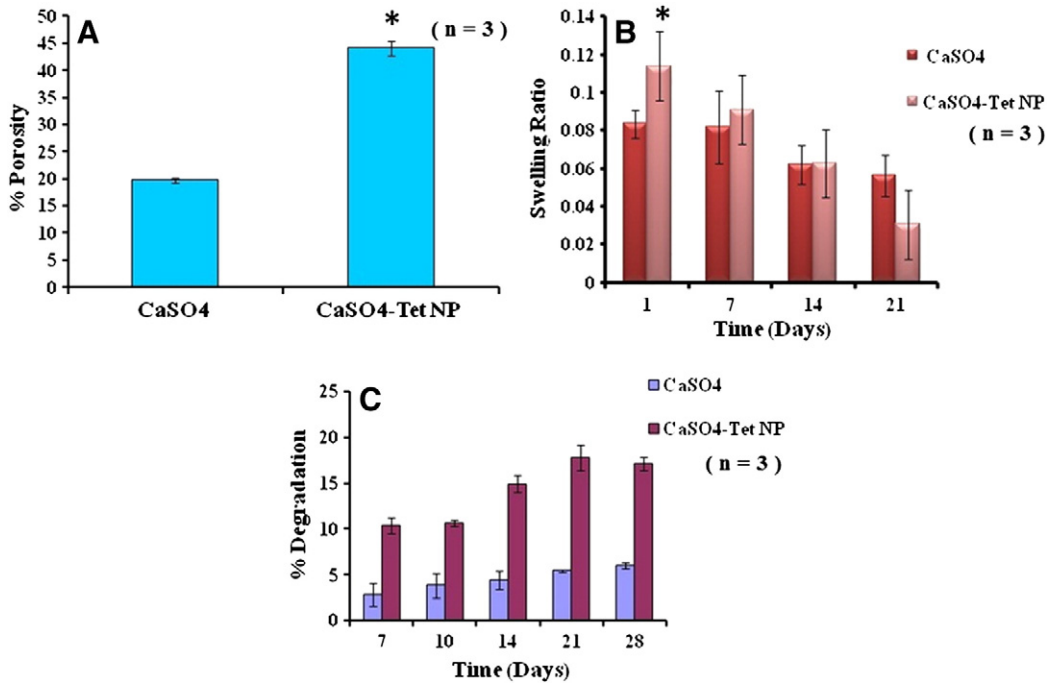

Fig. 3. (A) Porosity studies of $CaSO_4$ control and $CaSO_4$-Tet NP composite beads, (B) swelling studies of $CaSO_4$ control and $CaSO_4$-Tet NP composite beads in water, and (C) *in-vitro* degradation profile of $CaSO_4$ control and $CaSO_4$-Tet NP composite beads in PBS (* corresponds to $p < 0.05$ which is statistically significant).

7, 10, 14, 21 and 28, the NP incorporated composite beads showed a slightly higher degradation in comparison to the $CaSO_4$ control bead. At the end of the 28th day, 18% degradation was observed for the composite bead, however, the control $CaSO_4$ bead showed only 6% degradation.

3.4. In vitro drug release study and it's kinetic modeling

The drug release pattern (Fig. 4) showed a cumulative release of 27% from the $CaSO_4$-Tet NP composite beads at the end of 10 days following a sustained release pattern. The drug release data was fitted into various kinetic models such as zero order, first order, Higuchi model, and Hixson–Crowell model. The linearity of each plot was determined by the closeness of its regression coefficient to unity [29]. From the kinetic models (Fig. 5), the Higuchi model showed higher correlation value ($R^2 = 0.9279$) as compared to other models. Thus, the best fit model for the drug release is Higuchi model. In order to understand the drug release mechanism, the release data were fitted into Korsmeyer–Peppas model. The 'n' value of the Korsmeyer–Peppas model predicts that the mechanism of diffusion is non-Fickian in nature.

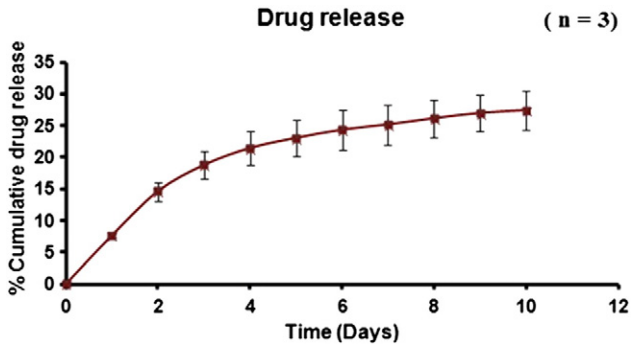

Fig. 4. *In vitro* drug release study showing percentage (%) cumulative drug released from $CaSO_4$-Tet NP composite beads measured for 10 days. Sustained release of Tet was observed.

3.5. Antibacterial activity and bacterial live dead assay

The results of antibacterial activity of $CaSO_4$ control and $CaSO_4$-Tet NP composite beads against *S. aureus* and *E. coli* bacteria as determined by serial dilution method are shown in Fig. 6. Experimental results depict the absence of bacterial colonies when treated with $CaSO_4$-Tet NP composite beads. This antibacterial activity could be attributed to the presence of Tet NPs in the composite bead.

Live/dead staining was used to identify the viable and nonviable bacterial cells in the LB medium containing $CaSO_4$ control and $CaSO_4$-Tet NP composite beads. The live cells were stained green with acridine orange and the dead cells were stained red with EtBr. The fluorescent images showed the majority of viable bacterial cells in the case of $CaSO_4$ control bead as well as in the *S. aureus* and *E. coli* negative controls (Fig. 7). However, non-viable bacterial cells were observed in the presence of $CaSO_4$-Tet NP composite beads.

3.6. Protein adsorption

The protein adsorption studies were carried out on $CaSO_4$ control and $CaSO_4$-Tet NP composite beads for 24 and 48 h respectively, wherein, the $CaSO_4$-Tet NP composite beads showed a significantly higher protein adsorption as compared to the control beads at both the time periods (Fig. 8A). Also maximum protein adsorption on the NP loaded composite bead was achieved in the initial 24 h period. Though a slight decrease in the adsorbed protein concentration on the NP loaded composite bead was observed in the 48 h period, the decrease was not statistically significant. This may be because of the fact that the maximum adsorption had already occurred within 24 h which would favor cell attachment and proliferation thereby decreasing the surface area available for further adsorption of proteins.

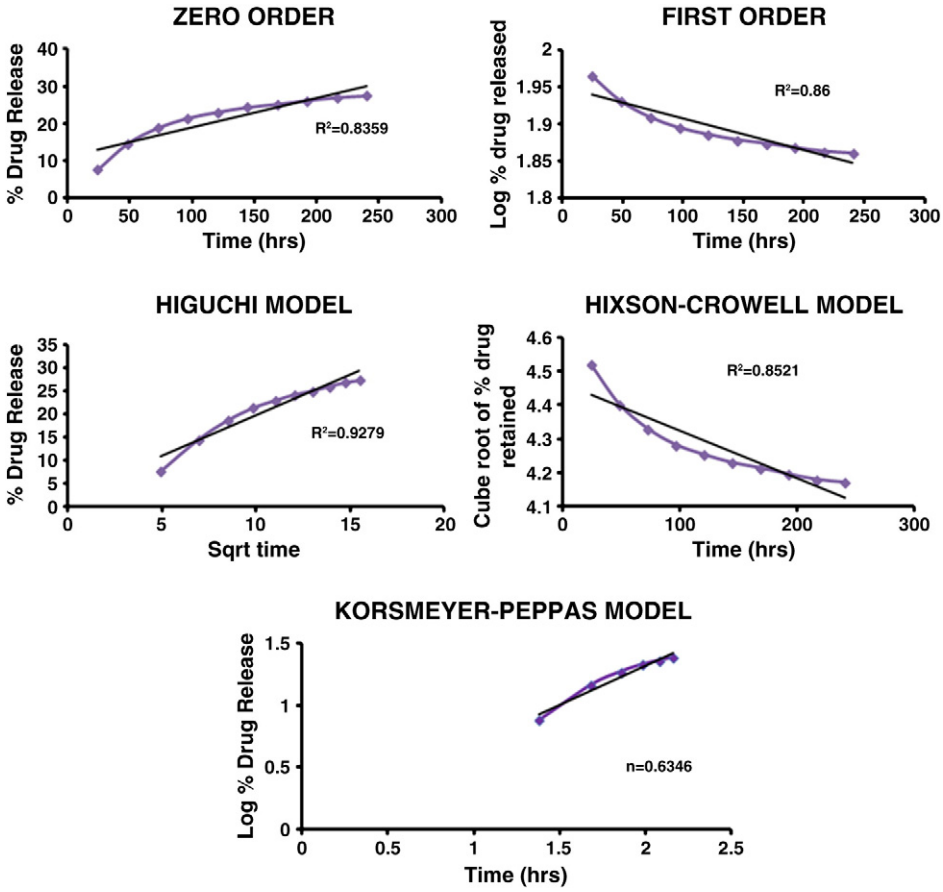

Fig. 5. *In vitro* drug release data fitted into various kinetic models. Higuchi model with higher regression coefficient ($R^2 = 0.9279$) is the best fit kinetic model. 'n' value of the Korsmeyer–Peppas model predicts non-Fickian diffusion mechanism.

3.7. Cell viability evaluation

The cytocompatibility of $CaSO_4$ control and $CaSO_4$-Tet NP composite beads was assessed using Alamar blue assay. The results (Fig. 8B) suggest that the viability of hPDL cells on both the control and NP loaded composite beads was comparable to the positive control (*i.e.* hPDL cells + serum containing media) at 24 and 48 h respectively.

3.8. Cell attachment and proliferation

The adhesion and morphology of hPDL cells on $CaSO_4$ control and $CaSO_4$-Tet NP composite beads was studied using SEM (Fig. 9A–D). The SEM images depicted that hPDL cells were attached and evenly spread throughout the surface of both the control and NP loaded composite beads. Initially the hPDL cells were rounded in appearance

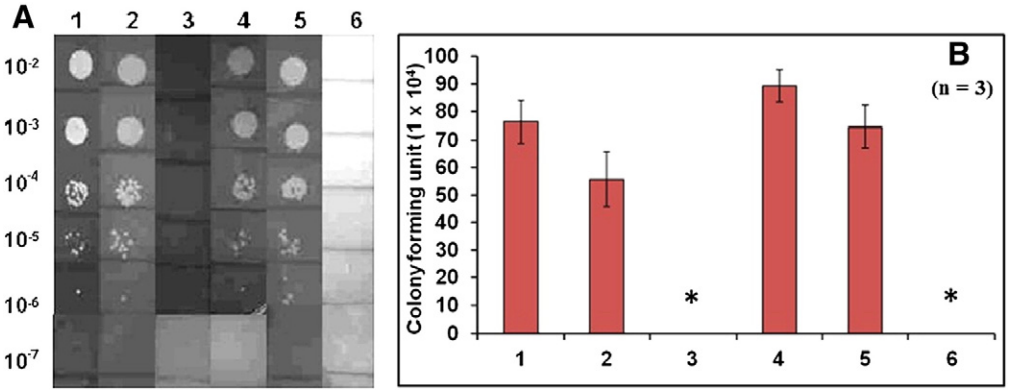

Fig. 6. (A) Images of antibacterial activity against (1) *S. aureus* negative control, (2) $CaSO_4$ control bead + *S. aureus*, (3) $CaSO_4$-Tet NP composite bead + *S. aureus*, (4) *E. coli* negative control, (5) $CaSO_4$ control bead + *E. coli*, (6) $CaSO_4$-Tet NP composite bead + *E. coli*. (B) Graphical representation of the antibacterial data as demonstrated in (A). (* corresponds to $p < 0.05$ which is statistically significant).

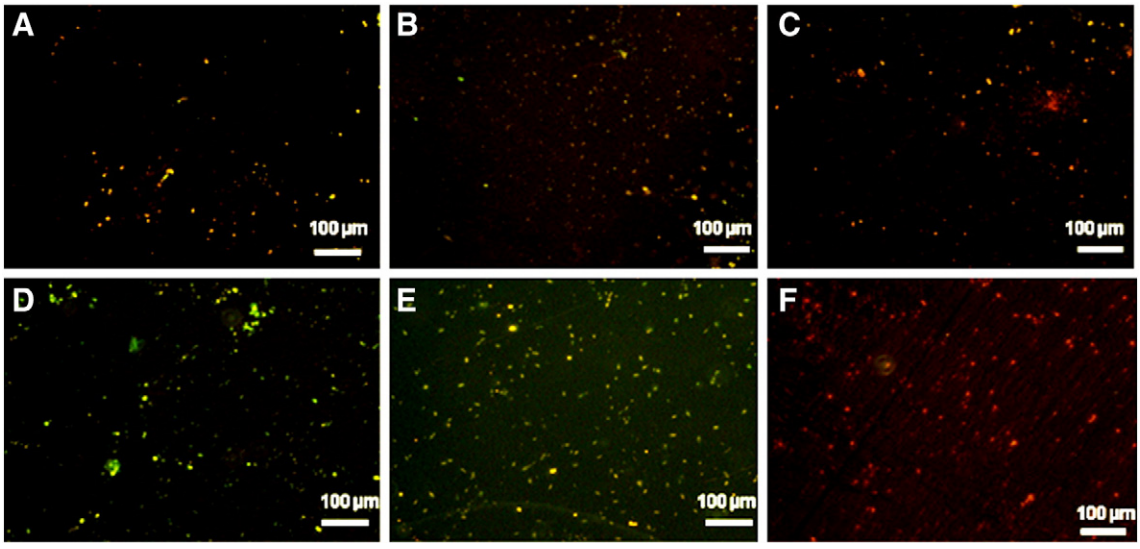

Fig. 7. Fluorescent images of bacterial live/dead assay (A) *S. aureus* negative control, (B) $CaSO_4$ control + *S. aureus*, (C) $CaSO_4$-Tet NP composite beads + *S. aureus*, (D) *E. coli* negative control, (E) $CaSO_4$ control + *E. coli*, (F) $CaSO_4$-Tet NP composite beads + *E. coli*.

followed by a well spread flattened morphology [32]. The flattening of the cells during spreading resulted in an increased porosity in the regions surrounding the cells.

DAPI staining was performed to study the proliferation and spreading of the hPDL cells on the $CaSO_4$ control and $CaSO_4$-Tet NP composite beads. Fluorescent images (Fig. 9E and F) of the stained beads showed that hPDL cells proliferated over the entire surface of both the control and composite beads.

3.9. Alkaline phosphatase (ALP) activity

Fig. 10 shows the ALP activity of the $CaSO_4$ control and $CaSO_4$-Tet NP composite beads after 7, 14 and 21 days. The hPDL cells cultured on the beads showed maximal ALP activity at 14 days followed by a decline in its activity thereafter.

4. Discussion

A localized antibiotic delivery system to the bacterial infection site is very beneficial as it allows achieving the required antibacterial effect and thus avoiding any systemic toxicity which is the main limitation of the conventional systemic delivery method. In our study a site specific local delivery system was fabricated wherein $CaSO_4$ loaded antibiotic nanoformulation would deliver the drug, tetracycline, locally at the infection site in a sustained manner thereby improving its bioavailability and providing the necessary antibacterial effect. In addition, the $CaSO_4$ bone cement would itself facilitate tissue regeneration.

Tet NPs were prepared using ionic gelation method with Ca^{2+} ions cross-linking the carboxyl group of *O*-CMC yielding Tet NPs. Encapsulating the Tet antibiotic into *O*-CMC polymeric vehicle has added advantage of sustained drug release, and improved drug bioavailability. Experimental outcomes indicated that the concentration of the polymeric solution and amount of drug have critical effects on the drug encapsulation within the polymer matrix [19]. Hence the polymer concentration was kept constant (0.1%) and the drug amount was varied. As the amount of drug increased beyond a certain amount (10:5 is the polymer:drug ratio), it showed a tendency to precipitate. Hence a polymer:drug ratio of 10:5 was chosen as the ideal concentration for further experimental study and the corresponding encapsulation and loading efficiency were calculated as 89% and 48%.

$CaSO_4$ control and $CaSO_4$-Tet NP composite beads were prepared and characterized using SEM, FTIR and XRD. The presence of Tet NPs in the composite beads was confirmed through characterization. Further, $CaSO_4$-Tet NP composite beads exhibited enhanced porosity, swelling and *in vitro* degradation properties in comparison to the $CaSO_4$ control. This enhancement could be attributed to the hydrophilic nature of *O*-CMC [38]. The presence of pores in the composite cement is essential as they would facilitate the encapsulation and uniform distribution of the Tet NPs rather than its presence being limited to the surface alone. Porosity and swelling properties also aid in tissue engineering by increasing the surface area which is the key feature required for the cells to attach to the beads; allow the supply of oxygen and other nutrients to the interior regions crucial for cellular migration, infiltration and proliferation [26]. Ideally for tissue engineering applications,

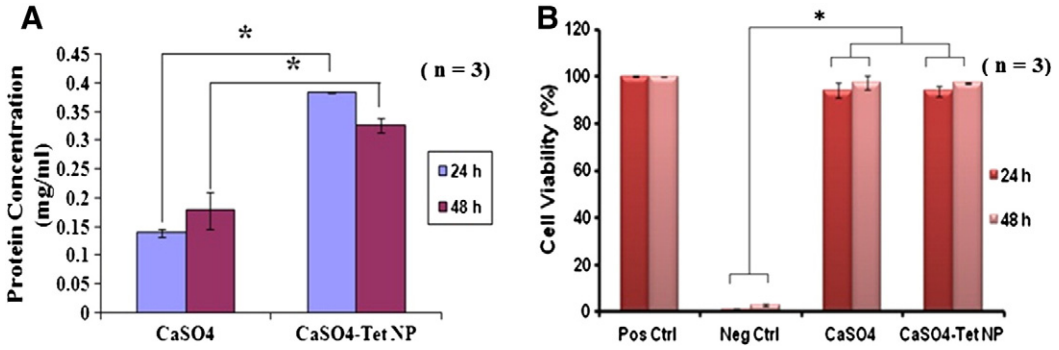

Fig. 8. (A) Protein adsorption on $CaSO_4$ control and $CaSO_4$-Tet NP composite beads, (B) hPDL cell viability on $CaSO_4$ control and $CaSO_4$-Tet NP composite beads [Pos Ctrl — hPDL cells + media, Neg Ctrl — hPDL cells + Triton] (* corresponds to $p < 0.05$ which is statistically significant).

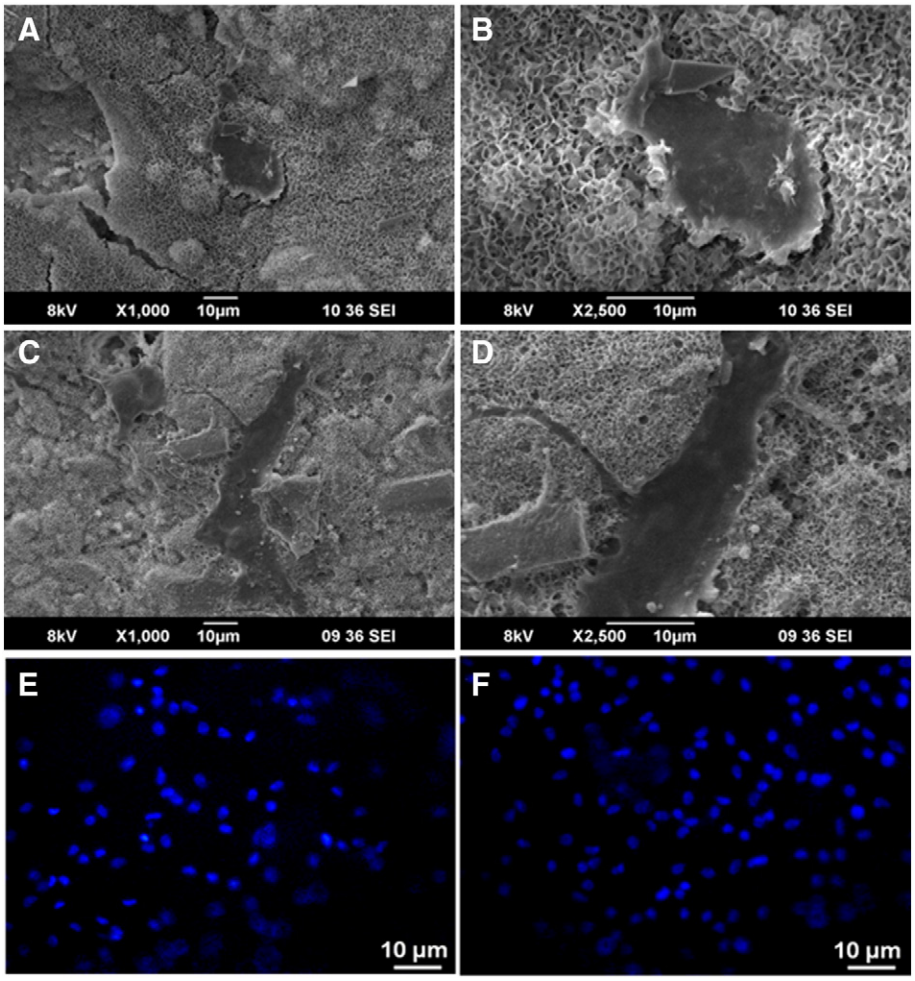

Fig. 9. SEM images of hPDL cell attachment (24 h) on (A, B) $CaSO_4$ control, (C, D) $CaSO_4$-Tet NP composite beads. DAPI stained fluorescent images of hPDL cell proliferation (48 h) on (E) $CaSO_4$ control and (F) $CaSO_4$-Tet NP composite beads.

the rate of degradation of a biomaterial should match the rate of new tissue formation [33]. Hence controlled swelling, porosity and degradation would be ideal for periodontal management.

Based on the analysis of drug release pattern from the composite bead, we may predict that as the composite bead degrades, the Tet NP on the surface may be released initially, following which we expect the release of the entrapped Tet NPs. The resorption property of the $CaSO_4$ cement is already well known [39]. Tet released from the NP carrier could be due to the lysis of the biodegradable polymer, or by the diffusion of the drug from the polymer, or due to the dissolution of the polymer by a linear process or could occur simultaneously [40], thereby releasing the drug. Reports suggest that Tet NPs are endocytosed by phagocytic cells and the colloidal carriers are degraded in endosomes by lysosomal esterases [19].

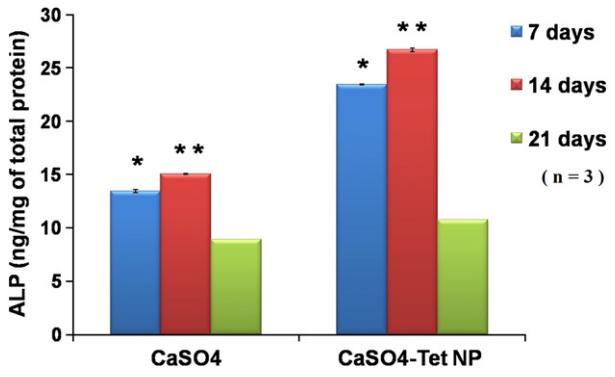

Fig. 10. ALP activity of hPDL cells on $CaSO_4$ control and $CaSO_4$-Tet NP composite beads (* corresponds to $p < 0.05$ and ** corresponds to $p < 0.01$ which are statistically significant).

The drug release kinetic studies predict that the release follows the Higuchi model wherein drug release is directly proportional to the square root of time and the release occurs at a slower rate as the distance of diffusion increases. Higuchi's model was designed based on Fick's laws of diffusion for drug embedded in porous matrix [41]. According to his model liquid penetrates the matrix and dissolves the embedded drug. As indicated earlier, the enhanced porosity, swelling and degradation results of the $CaSO_4$-Tet NP composite beads also enable better drug release from the system which is as described in the Higuchi model.

The $CaSO_4$-Tet NP composite beads exhibited antibacterial activity against both gram-positive *S. aureus* as well as gram-negative *E. coli* which was validated by serial dilution method and bacterial live/dead staining. Reports suggest that tetracycline is very effective against both gram-positive as well as gram-negative bacteria [37]. Based on the reports, it was presumed that as the $CaSO_4$-Tet NP composite beads degrade, the released Tet NPs would interact with the bacterial surface and the encapsulated Tet drug will be released. The prime mechanism of action of Tet in gram positive *S. aureus* and gram negative *E. coli* corresponds to the instantaneous widespread impairment of protein synthesis by interfering with the 30S ribosomal subunit of these bacteria [16,17]. In addition, bacterial cell division also ceases in the presence of the drug. The initial action could be bacteriostatic followed

by bactericidal [42]. Further studies are necessary to evaluate antibacterial activity against specific periopathogens such as *Actinobacillus actinomycetemcomitans*, *Porphyromonas gingivalis*, *Prevotella intermedia*.

Protein adsorption as estimated by BCA assay was enhanced in the $CaSO_4$-Tet NP composite beads as compared to the $CaSO_4$ control beads. This enhancement could be attributed to the presence of nanoparticles which increase the total surface area and binding sites for proteins or due to an electrostatic interaction between the material surface and the serum proteins. Protein adsorption further aids in cellular adhesion, infiltration and proliferation by the adsorption of adhesion molecules such as fibronectin and/or vitronectin [27,28]. Cytocompatibility of $CaSO_4$ control and $CaSO_4$-Tet NP composite beads was assessed by Alamar blue assay. Certain reports have indicated that the leachable products of $CaSO_4$ dissolution would produce an acidic microenvironment thereby trigger inflammation and affect the viability of normal cells and hamper tissue regeneration [43]. However, in our studies, no significant changes and alterations in hPDL cell viability were observed even on the addition of Tet NPs to the $CaSO_4$ cement. In addition to the cellular viability, hPDL cell attachment and proliferation results also confirmed the cytocompatible nature of the $CaSO_4$-Tet NP composite beads.

ALPase enzymatic activity is one of the chief and early biochemical markers of osteoblastic differentiation. Studies portray that hPDL cells reveal good ALP activity and thus also behave as osteoblasts. As seen from the ALP activity profile, the initial increase up to 14th day implies the completion of osteoblastic differentiation followed by a decrease thereafter indicating the onset of mineralization phase [44]. In addition, $CaSO_4$ cement along with their ionic and dissolution products would up-regulate gene expression in osteoprogenitor cells and give rise to rapid bone regeneration *in vivo* [8]. Hence the results showed good ALP activity of hPDL cells in the presence of osteogenic medium thus confirming its osteoblast-like behavior.

5. Conclusion

Overall the results demonstrated that the developed $CaSO_4$-Tet NP composite beads were biodegradable, cytocompatible and antibacterial in nature. In comparison to the reported literatures wherein bare antibiotics were used with bone cements, the amalgamation of antibiotic nanoformulation with the bone cement allowed sustained drug release and improved bioavailability with an uncompromised antibacterial effect. Another added advantage of the $CaSO_4$-Tet NP composite beads was that they could be applied locally at the infection site with lower drug dosage thus avoiding systemic toxicity. Thus, the $CaSO_4$-Tet NP composite beads could be effective in periodontal management.

Acknowledgements

The authors are grateful to SERB Division, Department of Science and Technology (DST), India, for providing the fund (Ref. No. SR/S1/OC-19/2012). The authors are also grateful to Nanomission, DST, India, which partially supported this work, under a “Thematic Unit of Excellence” grant. S. Sowmya acknowledges the Council of Scientific and Industrial Research (CSIR) for the financial support through Senior Research Fellowship (SRF-Award No. 9/963(0022)2K12-EMR-I). The authors are thankful to Annapoorna Mohandas, Smitha KT and Maya S for their valuable support and comments. The authors are also thankful to Mr. Sajin P. Ravi for his valuable help in SEM studies.

References

[1] A.K. Mane, A.P. Karmarkar, R.S. Bharadwaj, Anaerobic bacteria in subjects with chronic periodontitis and in periodontal health, J. Oral Health Community Dent. 3 (2009) 49–51.
[2] S. Sowmya, J.D. Bumgardener, K.P. Chennazhi, S.V. Nair, R. Jayakumar, Role of nanostructured biopolymers and bioceramics in enamel, dentin and periodontal tissue regeneration, Prog. Polym. Sci. 38 (2013) 1748–1772.
[3] J.T. Mader, G.C. Landon, J. Calhoun, Antimicrobial treatment of osteomyelitis, Clin. Orthop. 295 (1993) 87–95.
[4] W.A. Jiranek, A.D. Hanssen, A.S. Greenwald, Antibiotic-loaded bone cement for infection prophylaxis in total joint replacement, J. Bone Joint Surg. Am. 88 (2006) 2487–2500.
[5] G. Jenny, Local antibiotic therapy using gentamicin-PMMA chains in post-traumatic bone infections. Short and long-term results, Reconstr. Surg. Traumatol. 157 (1988) 36–46.
[6] G. Lewis, Properties of acrylic bone cement: state of the art review, J. Biomed. Mater. Res. 38 (1997) 155–182.
[7] A.V. Alt, T. Bechert, P. Steinrucke, M. Wagener, P. Seidel, E. Dingeldein, E. Domann, R. Schnettler, *In vitro* testing of antimicrobial activity of bone cement, Antimicrob. Agents Chemother. 48 (2004) 4084–4088.
[8] A.D. Hanssen, Local antibiotic delivery vehicles in the treatment of musculoskeletal infection, Clin. Orthop. Relat. Res. 437 (2005) 91–96.
[9] T.N. Gerhart, R.D. Roux, G. Horowitz, R.L. Miller, P. Hanff, W.C. Hayes, Antibiotic release from an experimental biodegradable bone cement, J. Orthop. Res. 6 (1988) 585–592.
[10] R.Z. LeGeros, Calcium phosphate-based osteoinductive materials, Chem. Rev. 108 (2008) 4742–4753.
[11] L.F. Peltier, E.Y. Bickel, R. Lillo, M.S. Thein, The use of plaster of Paris to fill defects in bone, Ann. Surg. 146 (1957) 61–69.
[12] E.M. Santschi, L. McGarvey, *In vitro* elution of gentamicin from plaster of Paris beads, Vet. Surg. 32 (2003) 128–133.
[13] D.E. Stabile, A.M. Jacobs, Development and application of antibiotic-loaded bone cement beads, J. Am. Podiatr. Med. Assoc. 80 (1990) 354–359.
[14] S. Gitelis, G.T. Brebach, The treatment of chronic osteomyelitis with a biodegradable antibiotic-impregnated implant, J. Orthop. Surg. 10 (2002) 53–60.
[15] G.G. Nicholas, J. Hanker, G. Ruff, S. Levin, The use of particulate hydroxyapatite and plaster of Paris in aesthetic and reconstructive surgery, Aesth. Plast. Surg. 17 (1993) 85–92.
[16] I. Chopra, M. Roberts, Tetracycline antibiotics: mode of action, applications, molecular biology, and epidemiology of bacterial resistance, Microbiol. Mol. Biol. Rev. 65 (2001) 232–260.
[17] I. Chopra, P.M. Hawkey, M. Hinton, Tetracyclines, molecular and clinical aspects, J. Antimicrob. Chemother. 29 (1992) 245–277.
[18] B.V.N. Nagavarma, H.K.S. Yadav, A. Ayaz, L.S. Vasudha, H.G.S. Kumar, Different techniques for preparation of polymeric nanoparticles: a review, Asian J. Pharm. Clin. Res. 5 (2012) 16–23.
[19] S. Maya, S. Indulekha, V. Sukhithasree, S.V. Nair, R. Jayakumar, R. Biswas, Efficacy of tetracycline encapsulated *O*-carboxymethyl chitosan nanoparticles against intracellular infections of *Staphylococcus aureus*, Int. J. Biol. Macromol. 51 (2012) 392–399.
[20] R. Jayakumar, K.P. Chennazhi, R.A.A. Muzzarelli, H. Tamura, S.V. Nair, N. Selvamurugan, Chitosan conjugated DNA nanoparticles in gene therapy, Carbohydr. Polym. 79 (2010) 1–8.
[21] L. Upadhyaya, J. Singh, V. Agarwal, R.P. Tewari, Biomedical applications of carboxymethyl chitosan, Carbohydr. Polym. 91 (2013) 452–466.
[22] N.D. Webb, J.D. McCanless, H.S. Courtney, J.D. Bumgardner, W.O. Haggard, Daptomycin eluted from calcium sulfate appears effective against *Staphylococcus*, Clin. Orthop. Relat. Res. 466 (2008) 1383–1387.
[23] A. Anitha, V.V. Divyarani, R. Krishna, V. Sreeja, N. Selvamurugan, S.V. Nair, H. Tamura, R. Jayakumar, Synthesis, characterization, cytotoxicity and antibacterial studies of chitosan, O-carboxymethyl and N, O-carboxymethyl chitosan nanoparticles, Carbohydr. Polym. 78 (2009) 672–677.
[24] A. Anitha, S. Maya, N. Deepa, K.P. Chennazhi, S.V. Nair, H. Tamura, R. Jayakumar, Efficient water soluble *O*-carboxymethyl chitosan nanocarrier for the delivery of curcumin to cancer cells, Carbohydr. Polym. 83 (2011) 452–461.
[25] A.C. Parker, J.K. Smith, H.S. Courtney, W.O. Haggard, Evaluation of two sources of calcium sulfate for a local drug delivery system: a pilot study, Clin. Orthop. Relat. Res. 469 (2011) 3008–3015.
[26] L. Jiang, Y. Li, X. Chengdong, Preparation and biological properties of a novel composite scaffold of nanohydroxyapatite/chitosan/carboxymethyl cellulose for bone tissue engineering, J. Biomed. Sci. 16 (2009) 65–75.
[27] S. Srinivasan, R. Jayasree, K.P. Chennazhi, S.V. Nair, R. Jayakumar, Biocompatible alginate/nano bioactive glass ceramic composite scaffolds for periodontal tissue regeneration, Carbohydr. Polym. 87 (2012) 274–283.
[28] P. Mathew, P.T.S. Kumar, N.S. Binulal, S.V. Nair, H. Tamura, R. Jayakumar, Development of novel α-chitin/nanobioactive glass ceramic composite scaffolds for tissue engineering applications, Carbohydr. Polym. 78 (2009) 926–931.
[29] S. Dash, P.N. Murthy, L. Nath, P. Chowdhury, Kinetic modeling on drug release from controlled drug delivery systems, Acta Pol. Pharm. 67 (2010) 217–223.
[30] P.T.S. Kumar, V.K. Lakshmanan, T.V. Anilkumar, C. Ramya, P. Reshmi, A.G. Unnikrishnan, S.V. Nair, R. Jayakumar, Flexible and microporous chitosan hydrogel/nano ZnO composite bandages for wound dressing: *in vitro* and *in vivo* evaluation, ACS Appl. Mater. Interfaces 4 (2012) 2618–2629.
[31] J.S. Braun, O. Hoffmann, M. Schickhaus, D. Freyer, E. Dagand, D. Bermpohl, T.J. Mitchell, I. Bechmann, J.R. Weber, Pneumolysin causes neuronal cell death through mitochondrial damage, Infect. Immun. 75 (2007) 4245–4254.
[32] K.T. Shalumon, S. Sowmya, D. Sathish, K.P. Chennazhi, S.V. Nair, R. Jayakumar, Effect of incorporation of nano bioactive glass and hydroxyapatite in PCL/chitosan nanofibers for bone and periodontal tissue engineering, J. Biomed. Nanotechnol. 9 (2012) 430–440.
[33] S. Sowmya, P.T.S. Kumar, V. Sreeja, S.V. Nair, K.P. Chennazhi, R. Jayakumar, Antibacterial and bioactive α- and β-chitin hydrogel/nanobioactive glass ceramic/nano silver composite scaffolds for periodontal regeneration, J. Biomed. Nanotechnol. 9 (2013) 1803–1816.
[34] F.B. de Sousa, M.F. Oliveira, I.S. Lula, M.T.C. Sansiviero, M.E. Cortes, R.D. Sinisterra, Study of inclusion compound in solution involving tetracycline and β-cyclodextrin by FTIR-ATR, Vib. Spectrosc. 46 (2008) 57–62.

[35] B. Salvadori, G.C. Capitani, M. Mellini, L. Dei, A novel method to prepare inorganic water-soluble nanocrystals, J. Colloid Interface Sci. 298 (2006) 487–490.
[36] C.R. Bhattacharjee, S.B. Paul, A. Nath, P.P.N. Choudhur, S. Choudhury, Synthesis, X-ray diffraction study and antimicrobial activity of calcium sulphate nanocomposites from plant charcoal, Materials 2 (2009) 345–352.
[37] A. Aurer, D. Plancak, Antimicrobial treatment of periodontal diseases, Acta Stomatol. Croat. 38 (2004) 67–72.
[38] V.K. Mourya, N.N. Inamdar, A. Tiwari, Carboxymethyl chitosan and its applications, Adv. Mater. Lett. 1 (2010) 11–33.
[39] R.M. Urban, T.M. Turner, D.J. Hall, N. Inoue, S. Gitelis, Increased bone formation using a calcium sulfate and calcium phosphate composite graft, Clin. Orthop. Relat. Res. 459 (2007) 110–117.
[40] L. Zhang, D. Pornpattananangkul, C.M.J. Hu, C.M. Huang, Development of nanoparticles for antimicrobial drug delivery, Curr. Med. Chem. 17 (2010) 585–594.
[41] W.I. Higuchi, Diffusional models useful in biopharmaceutics drug release rate processes, J. Pharm. Sci. 56 (1967) 315–324.
[42] J.H. Hash, M. Wishnick, P.A. Miller, On the mode of action of the tetracycline antibiotics in *Staphylococcus aureus*, J. Biol. Chem. 239 (1964) 2070–2078.
[43] M.A. Rauschmann, T.A. Wichelhaus, V. Stirnal, E. Dingeldein, L. Zichner, R. Schnettler, V. Alt, Nanocrystalline hydroxyapatite and calcium sulphate as biodegradable composite carrier material for local delivery of antibiotics in bone infections, Biomaterials 26 (2005) 2677–2684.
[44] E.K. Basdra, G. Komposch, Osteoblast-like properties of human periodontal ligament cells: an *in vitro* analysis, Eur. J. Orthod. 19 (1997) 615–621.